Ab Initio Molecular Orbital and RRKM Calculations of the Thermal Unimolecular Dissociation of the CH_2ClO Radical

Fuxiang Wu and Robert W. Carr*

Department of Chemical Engineering and Materials Science, University of Minnesota, Minneapolis, Minnesota 55455

Received: August 28, 2001; In Final Form: April 11, 2002

An ab initio molecular orbital study of the unimolecular elimination of HCl and Cl from the CH_2ClO radical is reported. Geometry optimizations were carried out at the HF/6-31G(d), MP2(full)/6-31G(d), and MP2(full)/6-31G(d,p) levels, and total energies were calculated using G2 and G2(MP2) theories. The zero-point-energy-corrected energy barrier for HCl elimination is predicted to be 8 kcal/mol, and for Cl elimination it is predicted to be 10.5 kcal/mol. RRKM models for both unimolecular reactions were made from the ab initio vibrational frequencies (scaled), moments of inertia and barrier heights. The RRKM predicted thermal rate coefficients for HCl elimination are in good agreement with experimental data taken over the temperature range 265−306 K and the pressure range 5−35 Torr (Wu, F.; Carr, R. W. *J. Phys. Chem.* A **2001**, *105*, 1423.) when the barrier height is adjusted to 8.5 kcal/mol. Because of the low energy barrier and, to a lesser extent, the small size of the reactant, the falloff curve is very broad, and the high pressure limit is predicted to be closely approached only when pressures of 10^7 Torr and above are reached. RRKM calculations of the rate coefficient for Cl elimination predict that this reaction is negligible compared with HCl elimination at moderate temperatures, but should be taken into account in high-temperature reactions. G2 theory predicts the 298 K enthalpy of formation of CH_2ClO to be -6.6 kcal mol^{-1}.

1. Introduction

Most theoretical investigations of the decomposition of halogenated methoxy radicals have dealt exclusively with bond scission reactions. MNDO semiempirical calculations of Cl and F atom elimination from $CCl_{3-x}F_xO$ radicals predict that Cl-atom extrusions have lower energy barriers than F atom extrusions, and should occur readily even at room temperature.[1−3] It has been found experimentally that C−Cl bond scission is facile if the oxy radical contains at least a second halogen atom, as with CCl_3O, $CFCl_2O$, CF_2ClO, CHFClO, and $CHCl_2O$ radicals.[4−9] The MNDO calculations of Rayez et al.[1] predict activation energies for unimolecular elimination of Cl from these radicals that are in the range of 9.7−12.4 kcal mol^{-1}, low enough to be in accord with the experimental observations.

In contrast with multiply halogenated methoxy radicals, experimental studies have not provided any evidence for C−Cl bond scission in CH_2ClO. Sanhueza and Heicklen[10] showed that CH_2ClO undergoes a bimolecular reaction with molecular oxygen, but no evidence for loss of Cl was reported. Niki et al.[11] also reported that CH_2ClO only reacts with O_2 in room-temperature air at 760 Torr, and Catoire et al.[12] found no evidence for Cl atoms from CH_2ClO in their 588 K experiments. MNDO calculations of Cl-atom elimination from CH_2ClO predict an activation energy of about 20 kcal mol^{-1},[1,12] but G2(MP2) calculations give a barrier height of only 11.2 kcal mol^{-1},[13] suggesting that Cl loss should be facile. However, Kaiser and Wallington[14] found experimental evidence for unimolecular elimination of HCl from CH_2ClO at 296 K, not C−Cl bond breaking. This reaction only becomes observable when the partial pressure of O_2 is decreased enough to make HCl elimination competitive with $CH_2ClO + O_2$. A subsequent study by Wallington et al.[15] reported the relative rate of HCl elimination and reaction of CH_2ClO with O_2 over the temperature range 264−336 K.

We have recently reported the kinetics of the reaction of CH_2ClO with O_2 and the unimolecular elimination of HCl at 306 K by observation of the kinetic growth of HC(O)Cl and HCl, two of the products of these competing reactions.[16] The unimolecular dissociation is well into the falloff in the 5−35 Torr pressure range of the experiments. The temperature dependence of the reactions of CH_2ClO with O_2 and NO, and the unimolecular elimination of HCl from CH_2ClO were subsequently studied from 265 to 306 K.[17] No experimental evidence for Cl atom elimination was found in either study. The rate coefficient for HCl elimination at 10 Torr can be expressed as $(7.7 \pm 2.3) \times 10^9 \exp[-(4803 \pm 722)/T]$ s^{-1}. The activation energy of 9.5 ± 1.4 kcal mol^{-1} at 10 Torr is in accord with the estimate of 8.6 ± 1.9 kcal mol^{-1} made by Wallington et al.,[15] but is significantly smaller than a MNDO prediction of 18.9 kcal/mol as the barrier for HCl elimination.[12]

In this work, high level ab initio molecular orbital calculations of CH_2ClO and of the transition states for elimination of HCl and atomic Cl were undertaken to gain further insight into reactions 1 and 2. Calculated values of the electronic barrier, and the reactant and transition state geometries and vibrational frequencies were taken as the basis of a RRKM

$$CH_2ClO \rightarrow HCO + HCl \quad (1)$$

$$CH_2ClO \rightarrow H_2CO + Cl \quad (2)$$

model for comparison of theory with experiment. Since the HCl elimination rate coefficients have been experimentally deter-

* To whom correspondence should be addressed.

10.1021/jp013326i CCC: $22.00
Published on Web 05/25/2002

mined only over the limited pressure and temperature range from 2 to 35 Torr[16,17] and from 265 to 306 K,[17] the RRKM model was used to extend k_1 over the entire range of atmospheric pressures and temperatures. The calculations have permitted an assessment the extent to which thermal unimolecular decomposition of CH_2ClO occurs in the atmosphere, in competition with removal by reaction with O_2.

$$CH_2ClO + O_2 \rightarrow HO_2 + HC(O)Cl \qquad (3)$$

The C−Cl bond breaking channel in CH_2ClO was also investigated by ab initio calculations and RRKM modeling to see if the calculations would confirm that the rate of reaction 2 is negligible at room temperature and below, to compare with other halogenated methoxy radicals, and to produce a kinetic model for use at higher temperatures where reaction 2 may be important.

2. Computational Method

2.1. Ab Initio Molecular Orbital Calculations. All ab initio molecular orbital calculations presented in this paper were carried out using the Gaussian 94 and Gaussian 98 series of programs[18,19] on a Silicon Graphics workstation or on an IBM SP supercomputer. Optimized geometries were first determined at the HF/6-31G(d) level, and then were fully optimized at the MP2(full)/6-31G(d) and MP2(full)/6-31G(d,p) levels using analytical gradients. For the geometry of the transition-state, the QST3 option was used to optimize a transition state structure based on the reactant, products, and an initial guess for the transition state. Vibrational frequencies were obtained at HF/6-31G(d) and MP2(full)/6-31G(d,p) levels using analytical second derivatives. The zero-point energies (ZPE's) for different species were also calculated at these levels. The frequency calculations verified that the located points were minima or first-order saddle points with no or, in the case of transition states, one imaginary frequency.

Total G2 and G2(MP2) energies were calculated using G2 theory[20] and G2(MP2) theory,[21,22] respectively. G2 theory is based on ab initio molecular orbital theory and MP2(full)/6-31G(d) geometries using all electrons. Total G2 energies were calculated at the complete fourth-order Møller−Plesset perturbation theory [MP4SDTQ/6-311G(d,p)] with corrections from higher level calculations. The corrections include the following terms: (a) A correction for diffuse functions: $\Delta E(+) =$ E[MP4/6-311+G(d,p)] − E[MP4/6-311G(d,p)]. (b) A correction for higher polarization functions on non-hydrogen atoms: $\Delta E(2df) = E$[MP4/6-311G(2df,p)] − E[MP4/6-311G(d,p)]. (c) A correction for inclusion of a third d function on non-hydrogen atoms and a second p function on hydrogens: $\Delta =$ E[MP2/6-311+G(3df,2p) − E[MP2/6-311G(2df,p)] − E[MP2/6-311+G(d,p)] + E[MP2/6-311G(d,p)]. (d) A correction for correlation effects beyond fourth-order perturbation theory: $\Delta E(QCI) = E$[QCISD(T)/6-311G(d,p)] − E[MP4/6-311G(d,p)]. (e) A higher level correction to account for remaining basis set deficiencies: $HLC = -Bn_\alpha - An_\beta$, where $A = 4.81$ mHartree, $B = 0.19$ mHartree, and n_α and n_β are the number of alpha and beta electrons, respectively, with $n_\alpha \geq n_\beta$. (f) Zero-point energy correction, E(ZPE), obtained from HF/6-31G(d) optimized frequencies scaled by the factor 0.8929. The resulting total G2 energy is given by $E_{0,G2} = E$[MP4/6-311G(d,p)] + $\Delta E(+)$ + $\Delta E(2df)$ + Δ + $\Delta E(QCI)$ + HLC + E(ZPE).

G2(MP2) theory is one of the two variations of G2 theory. In G2(MP2) theory the basis- set extensions are replaced by a single correction obtained using second-order Møller−Plesset perturbation theory (at the MP2 level): $\Delta_{MP2} = E$[MP2/6-311+G(3df,2p)] − E[MP2/6-311G(d,p)]. Therefore, it provides substantial savings in computational time.

The total G2(MP2) energy is given by

$$E_{0,G2(MP2)} = E[\text{QCISD(T)/6-311G(d,p)}] + \Delta_{MP2} + \text{HLC} + E(\text{ZPE})$$

It has been found that the average absolute deviation between energy quantities calculated at the G2 level of theory and experimental measurements is 1.21 kcal/mol from 125 test cases, while for G2(MP2) theory the deviation was 1.58 kcal/mol.[21]

2.2. RRKM Calculations. Rate coefficients for the unimolecular elimination of HCl and Cl from CH_2ClO were calculated from RRKM theory, using the vibrational frequencies, moments of inertia, and critical energies (ZPE barrier heights) from the ab initio calculations as input data. Since the total energies are based on MP2(Full)/6-31G(d,p) optimized geometries, in the RRKM calculations the vibrational frequencies were scaled by a factor of 0.9427.[19] The UNIMOL Fortran program package[23] was used for calculations of the pressure and temperature dependence of the thermal unimolecular rate coefficients. The UNIMOL suite of programs includes two separate main programs. The first, called RRKM, carries out microcanonical rate coefficient calculations, computes high-pressure limit rate parameters and also gives strong collision values for both k_∞ and k_0. It also generates a file containing all data which will be subsequently used in the solution of the master equation. The second program, MASTER, gives a numerical solution of the master equation with energy transfer described by the biased random walk model. It computes the low-pressure limit rate coefficient, the collisional efficiency (β), and it can compute a complete falloff curve around a median pressure. The detailed calculation method and basic theory used by this program are given by Gilbert et al.[23,24] The "tight" transition state treatment and a reaction path degeneracy of 2 were used for the HCl elimination calculations. The RRKM calculations were done on the Silicon Graphics workstation.

The Lennard-Jones collision diameters and well depths needed to calculate the collision frequency, ω, were estimated from $\sigma_{AB} = (\sigma_{oxy} + \sigma_{mix})/2$, where σ_{oxy} is for the CH_2ClO radical, estimated to be 4.38 Å, and σ_{mix} is for the gas mixture. The typical gas mixture consists 15% Cl_2, 25% CH_3Cl and 60% N_2. With $\sigma_{N_2} = 3.9$ Å, $\sigma_{Cl_2} = 4.3$ Å and $\sigma_{CH_3Cl} = 4.43$ Å, σ_{AB} was calculated to be 4.24 Å. The Lennard-Jones well depth, $\epsilon_{AB}(K)$, given by $\epsilon_{AB}(K) = [\epsilon_{oxy}(K)\ \epsilon_{mix}(K)]^{1/2}$, is equal to 219 K using $\epsilon_{oxy} = 280$ K and $\epsilon_{mix} = 170$ K.

The use of ab initio computed moments of inertia, vibrational frequencies, and critical energies, constitute an RRKM model for $k(E)$ with no adjustable parameters. The biased random-walk model, with Lennard-Jones parameters from the literature, provides a collisional deactivation model that can also be employed without adjustment.

3. Results

3.1. Ab initio Calculations. Calculations were carried out for the dissociation of CH_2ClO into HCl and HCO (reaction 1), and Cl and H_2CO (reaction 2). These are the two lowest energy decomposition channels of CH_2ClO, and the only ones that need to be considered in atmospheric chemistry.

Transition states for reactions 1 and 2 were located. Geometry optimization of the reactant, the transition states and the products were done at HF/6-31G(d), MP2(full)/6-31G(d), and MP2(full)/6-31G(d,p) levels. Attempts to obtain an optimized geometry

TABLE 1: Optimized Geometries for the Unimolecular Elimination of HCl and Cl from CH_2ClO

	bond length (angstroms)					
	C−O	C−H_1	C−H_2	C−Cl	H−Cl	ref
reactants						
CH_2ClO ($\tilde{X}^2A''$)	1.3499	1.0920	1.0920	1.7946		this work[a]
	1.3499	1.0966	1.0966	1.7965		this work[b]
	1.34	1.11	1.11	1.83		ref 12[c]
	1.350	1.096	1.096	1.797		ref 13[b]
CH_2ClO ($\tilde{A}^2A'$)	1.3873	1.0927	1.0927	1.7811		this work[b]
TS (−HCl) (^2A)	1.2050	1.0896	1.1420	2.1081		this work[a]
	1.23	1.11	1.18	2.04		ref 12[c]
TS (−Cl) (^2A)	1.24915	1.09247	1.09246	2.15104		this work[a]
	1.24997	1.09696	1.09688	2.15236		this work[b]
	1.24	1.11	1.11	2.27		ref 12[c]
	1.250	1.097	1.097	2.152		ref 13[b]
products						
$CH_2(O)$ ($\tilde{X}^1A_1$)	1.2195	1.0994	1.0994			this work[a]
	1.22	1.104	1.104			ref 13[b]
HC(O) ($\tilde{X}^2A'$)	1.1911	1.1173				this work[a]
	1.191	1.123				ref 13[b]
HCl ($\tilde{X}^1\Sigma^+$)					1.2682	this work[a]
					1.280	ref 13[b]

	planar and dihedral angles (degrees)					
	H_1−C−Cl	H_2−C−Cl	O−C−Cl	H_1−C−Cl−O	H_2−C−Cl−O	ref
reactants						
CH_2ClO ($\tilde{X}^2A''$)	107.63	107.63	115.25	121.27	−121.27	this work[a]
	107.67	107.67	115.11	121.20	−121.20	this work[b]
	106.3	106.3	111.9	120.7	−120.7	ref 12[c]
	108.5	108.5	115.1			ref 13[b]
CH_2ClO ($\tilde{A}^2A'$)	107.96	107.96	103.98	119.41	−119.41	this work[b]
TS (−HCl) (^2A)	100.51	67.70	117.43	140.33	−108.15	this work[a]
	104.7	67.0	114.6	139.7	−113.0	ref 12[c]
TS (−Cl) (^2A)	97.6002	97.6019	90.56	121.26	−121.26	this work[a]
	97.7480	97.6454	90.36	121.18	−121.20	this work[b]
	98.1	98.2	84.9	122.1	−122.1	ref 12[c]
			90.4			ref 13[b]
products						
$H_2C(O)$ ($\tilde{X}^1A_1$)	H_1−C−O	H_2−C−O	H_1−C−O−H_2			
	122.24	122.24	180.0			this work[a]
	122.2	122.2				ref 13[b]
HC(O) ($\tilde{X}^2A'$)	H−C−O					
	123.57					this work[a]
	123.3					ref 13[b]

[a] Optimized at MP2(full)/6-31G(d,p). [b] Optimized at MP2(full)/6-31G(d). [c] From MNDO calculations.

for the HCl elimination transition state at the MP2(Full)/6-31G(d) level failed. To find the HCl elimination transition state it was necessary to do geometry optimizations at the MP2(Full)/6-31G(d,p) level of theory. Thus for reaction 1, the total energies, including the G2 and G2(MP2) energies of the reactant, the transition states, and the reaction products, were calculated on MP2(full)/6-31G(d,p) optimized geometries for all species. Vibrational frequency calculations, done on each of the transition states at HF/6-31G(d), MP2(full)/6-31G(d,p) and MP2(full)/6-31G(d) levels (the last for C−Cl only), have one imaginary frequency confirming that the optimized structures are transition states for HCl and Cl elimination from CH_2ClO.

Reaction path calculations (IRC calculations) were performed for HCl elimination at MP2(full)/6-31G(d,p), and Cl elimination at HF/6-31G(d) and MP2(full)/6-31G(d) using the Gaussian 98 reaction path following facility. The IRC calculations showed that for each transition state the reverse reaction path leads toward the CH_2ClO ground state as total energy decreases. Similarly, the HCl elimination transition state leads toward the ground states of HCl and HCO, and the C−Cl bond scission transition state leads toward the ground states of Cl and H_2CO.

Optimized geometries for CH_2ClO, the transition states and the reaction products are listed in Table 1. The numerical values were obtained by reading corresponding molecular structures displayed by a visualization package of Gaussian 98, GaussianView. Also listed, for comparison, are the corresponding bond

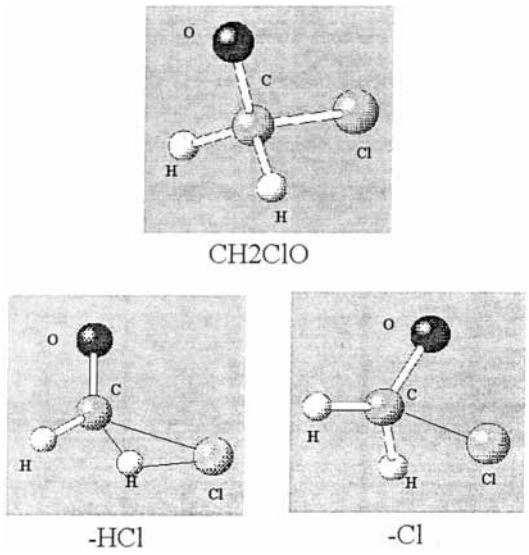

Figure 1. Reactant and transition state structures for HCl and Cl-atom elimination from CH_2ClO.

TABLE 2: ZPE Corrected Total Energies and Parameters (Unit: hartree)

HCl Elimination, Optimized Geometry at MP2(full)/6-31G(d,p)

	CH_2ClO	TS	HCl	HC(O)
MP4/6-311G(d,p)	−573.836 81	−573.812 98	−460.256 27	−113.606 05
MP4/6-311+G(d,p)	−573.845 68	−573.821 47	−460.257 09	−113.611 81
MP4/6-311G(2df,p)	−573.954 37	−573.933 13	−460.311 91	−113.663 15
MP2/6-311+G(3df,2p)	−573.915 44	−573.890 54	−460.292 28	−113.647 80
MP2/6-311G(2df,p)	−573.895 80	−573.871 72	−460.284 77	−113.635 20
MP2/6-311+G(d,p)	−573.798 03	−573.771 20	−460.238 21	−113.586 23
MP2/6-311G(d,p)	−573.789 88	−573.763 34	−460.237 53	−113.580 72
QSISD(T)/6-311G(d.p)	−573.839 43	−573.824 97	−460.256 83	−113.603 70
no. of α valence electrons	10	10	4	6
no. of β valence electrons	9	9	4	5
ZPE(HF/6-31G(d))*	0.032 317	0.022 911	0.007 258	0.014 384
G2(MP2)	−574.010 17	−573.997 36	−460.331 59	−113.695 98
G2	−574.022 54	−574.009 76	−460.340 13	−113.698 85

Cl Elimination, Optimized Geometry at MP2(full)/6-31G(d,p)

	CH_2ClO	TS	Cl	$H_2C(O)$
MP4/6-311G(d,p)	−573.836 81	−573.790 18	−459.602 63	−114.236 49
MP4/6-311+G(d,p)	−573.845 68	−573.797 78	−459.603 77	−114.243 11
MP4/6-311G(2df,p)	−573.954 37	−573.911 78	−459.656 29	−114.295 37
MP2/6-311+G(3df,2p)	−573.915 44	−573.869 64	−459.633 38	−114.280 11
MP2/6-311G(2df,p)	−573.895 80	−573.851 60	−459.629 00	−114.265 13
MP2/6-311+G(d,p)	−573.798 03	−573.748 21	−459.586 16	−114.215 43
MP2/6-311G(d,p)	−573.789 88	−573.741 36	−459.585 14	−114.208 94
QSISD(T)/6-311G(d.p)	−573.839 43	−573.794 39	−459.603 29	−114.234 89
no. of α valence electrons	10	10	4	6
no. of β valence electrons	9	9	3	6
ZPE(HF/6-31G(d))*	0.032 317	0.029 917	0.0	0.029 201
G2(MP2)	−574.010 17	−573.993 43	−459.666 72	−114.336 06
G2	−574.022 54	−574.005 96	−459.676 63	−114.338 91

Cl Elimination, Optimized Geometry at MP2(full)/6-31G(d)

	CH_2ClO	TS	Cl	$H_2C(O)$
MP4/6-311G(d,p)	−573.836 89	−573.789 89	−459.602 63	−114.23656
MP4/6-311+G(d,p)	−573.845 76	−573.797 50	−459.603 77	−114.243 19
MP4/6-311G(2df,p)	−573.954 45	−573.911 46	−459.656 29	−114.295 42
MP2/6-311+G(3df,2p)	−573.915 42	−573.869 23	−459.633 38	−114.280 09
MP2/6-311G(2df,p)	−573.895 82	−573.851 23	−459.629 00	−114.265 12
MP2/6-311+G(d,p)	−573.798 06	−573.747 85	−459.586 16	−114.215 44
MP2/6-311G(d,p)	−573.789 91	−573.740 99	−459.585 14	−114.208 96
QSISD(T)/6-311G(d.p)	−573.839 52	−573.794 10	−459.603 29	−114.234 95
no. of α valence electrons	10	10	4	6
no. of β valence electrons	9	9	3	6
ZPE(HF/6-31G(d))[a]	0.032 317	0.029 917	0.0	0.029 201
G2(MP2)	−574.010 22	−573.993 47	−459.666 72	−114.336 08
G2	−574.022 59	−574.006 00	−459.676 63	−114.338 92

[a] Unscaled zero-point energy. Scale factor of 0.8929 is used for ZPE correction.

lengths and angles from the MNDO calculations of Catoire et al.[12] and G2(MP2) calculations at MP2(full)/6-31G(d) of Wang et al. for C−Cl bond scission.[13] The images of MP2(full)/6-31G(d,p) optimized structures of CH_2ClO and the transition states for HCl and Cl-atom elimination, which were also created by GaussianView, are shown in Figure 1. The calculated ground-state total energies at different levels of theory, and other parameters for calculating total G2 energy and total G2(MP2) energy, are listed in Table 2. The total energies listed in Table 2 are HF/6-31G(d) ZPE corrected with scale factor of 0.8929. The unscaled MP2(full)/6-31G(d,p) vibrational frequencies, and moments of inertia for reactant and transition states are listed in Table 3.

In the geometry optimization calculations at MP2(full)/6-31G(d), two structures of CH_2ClO were found, the $^2A''$ ground state, and a $^2A'$ excited state. Their G2 and G2(MP2) energies differed by 6.98 and 6.93 kcal/mol, respectively. Both are stable structures. In addition, CI−Singles (CIS) calculations for modeling excited states as combinations of single substitutions out of the Hartree−Fock ground state of CH_2ClO were done. The CIS calculations found, at the HF/6-31G(d) level, four excited states with predicted energies of 0.573 eV, 4.856, 7.515, and 7.714 eV. The 13.2 kcal/mol excitation energy of the lowest excited state at this lower level of theory is larger than the approximately 6.95 kcal/mol difference found for the two CH_2ClO structures calculated at the G2 and G2(MP2) levels. Discussion of the role of the excited state is in section 4.

The HCl elimination transition state is an unsymmetrical structure and thus is a ^2A electronic state. When geometry optimization of the C−Cl bond scission transition state was attempted from an initial guess in which the structure had C_S symmetry, as does the CH_2ClO reactant, the program did not converge. Convergence was only obtained when an unsymmetrical structure was taken for the initial guess. The converged structure shows that the asymmetry comes from the two C−H bond lengths and H−C−Cl angles, which are different. In a structure having C_S symmetry these distances and angles would be the same. When optimizations were done at MP2 with the 6-31G(d,p) basis set, asymmetry was due to only a slight difference in the C−H bond length. This difference was

TABLE 3: Unscaled Vibrational Frequencies and Moments of Inertia (Calculated from MP(full)/6-311(d,p) Optimized Geometries)

	vibrational frequencies (cm^{-1})
reactant (CH_2ClO)	411, 725, 751, 1125, 1128, 1381, 1435, 3107, 3179
transition state for HCl elimination	1920 i, 353, 411, 925, 1148, 1394, 1518, 2557, 3178
transition state for Cl elimination	737 i, 265, 770, 1066, 1268, 1448, 1644, 3098, 3202
	principal moments of inertia ($Å^2$)
reactant (CH_2ClO)	94.830, 87.370, 10.651
transition state for HCl elimination	111.203, 104.884, 9.273
transition state for Cl elimination	96.547, 85.627, 14.374
	rotational constant (cm^{-1})
reactant (CH_2ClO)	0.1778, 0.1930, 1.5829
transit state for HCl elimination	0.1516, 0.1505, 1.8180
transition state for Cl elimination	0.1746, 0.1969, 1.1730

somewhat larger with the 6-31G(d) basis set. The electronic state of the C−Cl transition state predicted by this level of theory is thus ^2A.

The barrier heights for forward and reverse HCl and Cl-atom elimination reactions were calculated from the ZPE corrected total QCISD(T)/6−311(d,p), MP4/6-311G(2df,p), G2(MP2), and G2 energies listed in Table 2, and are presented in Table 4. The forward barrier is relative to the ground state of CH_2ClO in all calculations. To evaluate the effect of scale factor on the calculated total energies and the critical energies at the G2 level, the calculations were done using scale factors of 0.8929 and 0.9135, the suggested scale factors for the vibrational frequencies and ZPE, respectively.[18] The effect of the scale factors on the barrier height calculation was found to be insignificant, and 0.8929 was used as a common scale factor for frequency and energy calculations without appreciable error.

The energy barriers at the QCISD(T)/6-311G(d,p) and the MP4/6-311G(2df,p) level are significantly higher than the G2 and G2(MP2) barriers. Figure 2 diagrams the G2 and G2(MP2) energies of the two transition states and the two sets of products

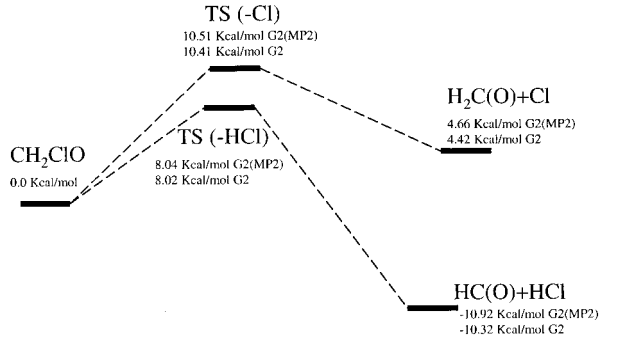

Figure 2. Reaction barrier heights for HCl and Cl-atom elimination calculated from total G2 and G2(MP2) energies.

relative to the ground-state energy of CH_2ClO, arbitrarily taken as zero. The highest levels of calculation predict a barrier height of 8 kcal/mol for HCl-elimination from CH_2ClO, and a barrier height of 10.4 kcal/mol (G2) or 10.5 kcal/mol (G2MP2) for Cl-atom elimination. The calculated energy barriers in Table 4 also show that the optimized geometries of the transition state for Cl elimination determined at MP2(full)/6-31G(d,p) and MP2(full)/6-31G(d) have an insignificant effect on the determination of the energy barrier. For example, the G2 energy barrier for Cl elimination changed from 10.40 kcal/mol (MP2(full)/6-31G(d,p)) to 10.41 kcal/mol (MP2(full)/6-31G(d)).

As a check on the G2(MP2) and G2 calculations, total energies of the products of reactions 1 and 2 were calculated for comparison with the literature. The total energies are in excellent agreement with values that have been reported in the literature.[13,20,22] However, the G2(MP2) total energy of CH_2ClO reported by Wang et al.[13] is smaller than our G2(MP2) calculation by 0.53 kcal/mol, and their transition state energy for C−Cl bond breaking is 0.16 kcal/mol larger than ours. These differences account for the different G2(MP2) C−Cl barriers reported; 10.5 kcal/mol (this work) and 11.2 kcal/mol.[13] We have been unable to determine the reason(s) for the discrepancies in CH_2ClO and transition state energies. The 0.53 kcal/mol discrepancy in ground-state energy is too small to be accounted for by different electronic states since the $^2A'$ state of CH_2ClO is predicted to be nearly 7 kcal/mol above the $^2A''$ ground state.

There is spin contamination in the calculations. For the CH_2ClO radical $\langle S^2 \rangle = 0.758$, only slightly larger than the

TABLE 4: Calculated Energy Barriers (Kcal/Mol)

HCl Elimination

optimization	energy level	ZPE[a]	forward reaction	reverse reaction
MP2(full)/6-31G(d,p)	QSISD(T)/6-311G(d.p)	HF/6-31G(d)	9.07	22.32
	MP4/6-311+G(2df,p)	HF/6-31G(d)	13.32	26.31
	G2(MP2)	HF/6-31G(d)	8.04	18.96
	G2	HF/6-31G(d)	8.02	18.34

Cl Elimination

optimization	energy level	ZPE[a]	forward reaction	reverse reaction
MP2(full)/6-31G(d,p)	QSISD(T)/6-311G(d.p)	HF/6-31G(d)	11.32	10.54
	MP4/6-311+G(2df,p)	HF/6-31G(d)	14.60	12.90
	G2(MP2)	HF/6-31G(d)	10.51	5.87
	G2	HF/6-31G(d)	10.40	6.01

Cl Elimination

optimization	energy level	ZPE[a]	forward reaction	reverse reaction
MP2(full)/6-31G(d)	QSISD(T)/6-311G(d.p)	HF/6-31G(d)	11.32	10.52
	MP4/6-311+G(2df,p)	HF/6-31G(d)	14.62	12.90
	G2(MP2)	HF/6-31G(d)	10.51	5.85
	G2	HF/6-31G(d)	10.41	5.99

[a] Scale factor of 0.8929 is used for ZPE correction.

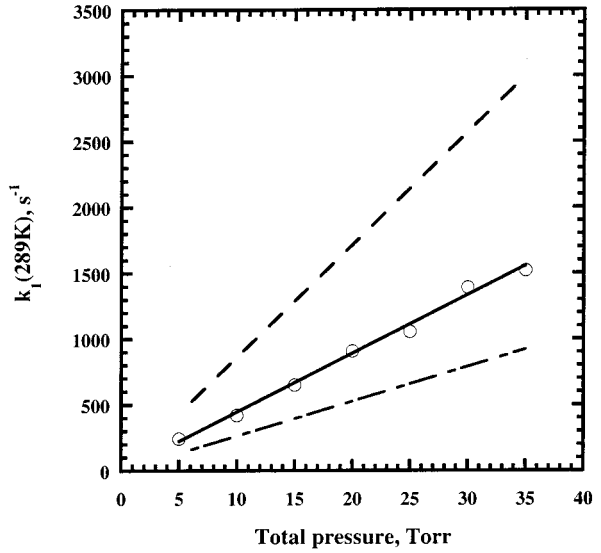

Figure 3. A comparison of experimental and RRKM calculated values of k_1 at 289 K.) Experimental results. Lines represent RRKM results with different critical energies. (—) $E_0 = 8.5$ kcal mol^{-1}. (– –) $E_0 =$ 8.0 kcal mol^{-1}. (· –) $E_0 = 9.0$ kcal mol^{-1}.

expected value of $\langle S^2 \rangle = 0.75$ for doublets. But for the C−Cl bond breaking transition state at QCISD(T)/6-311G(d,p), $\langle S^2 \rangle = 0.930$, and for the HCl elimination transition state at the same level $\langle S^2 \rangle = 0.92$. However, the good agreement between theoretical and experimental values of k_1 presented below suggests that spin contamination may not significantly affect the energy calculations, at least for this channel.

3.2. RRKM Calculations. RRKM calculations of the rate coefficient for HCl elimination were done for comparison with the experimentally determined rate coefficients.[16,17] The experimental data are the pressure dependence of k_1 from 5 to 35 Torr at 289 and 306 K, and the 10 Torr rate coefficients at 265, 280, 289, and 306 K. The moments of inertia, scaled vibrational frequencies from the MP2(Full)/6-31G(d,p) geometry optimizations, and the G2 and G2(MP2) barrier heights constitute the basic elements of the RRKM model. Microcanonical rate coefficients were computed from these elements. The biased random-walk model for collisional energy transfer was used for calculation of thermal rate coefficients.

Figure 3 shows a comparison of the pressure dependence of k_1 at 289 K with RRKM calculations. When the G2 and G2(MP2) barriers are rounded off to 8.0 kcal/mol the computed rate coefficients are significantly larger than experiment, but the data can be very well fit with a barrier of 8.5 kcal mol^{-1}, everything else in the RRKM model remaining unchanged. A good RRKM fit to the 306 K pressure dependence of k_1 was also found with the 8.5 kcal mol^{-1} barrier. The adjustment of the barrier height is justified since, as shown next, the experimental data are very close to the low-pressure limit.

The linearity of the 289 K k_1 vs pressure data suggest that they are closely approaching the low-pressure limit. The low-pressure limit rate coefficient is given by $k_{1,0} = \lim_{[m]\to 0}(k_1/[M])$. If this expression is used to estimate $k_{1,0}$ from the slope of the experimental data points in Figure 3, $k_{1,0} = 1.23 \times 10^{-15}$ cm^3 molecule^{-1} s^{-1} is obtained. The RRKM calculated low-pressure limit is $k_{1,0}(\text{calcd}) = 1.24 \times 10^{-15}$ cm^3 molecule^{-1} s^{-1}, showing that the data are for all practical purposes at the low-pressure limit. The RRKM expression for $k_{1,0}$ contains the collisional energy transfer parameters and E_0 as the only model dependent quantities.[25] With a specified collision model E_0 is the only model dependent parameter.

TABLE 5: A Comparison of k_3 Determined by Experiment and Calculation at 289 K

		k_1 (s^{-1})		
pressure (Torr)	exptl	$E_0 = 8.0$ (kcal/mol)	$E_0 = 8.5$ (kcal/mol)	$E_0 = 9.0$ (kcal/mol)
5	244 ± 38	429	222	131
8	419 ± 117	858	445	263
15	650 ± 117	1290	667	394
20	907 ± 41	1720	889	525
25	1055 ± 275	2140	1110	656
30	1392 ± 25	2570	1330	788
35	1521 ± 260	3000	1560	919
700	- - - -	59600	19600	18100

Figure 3 shows that an upward adjustment in E_0 of only 0.5 kcal/mol is required to fit the data. This is well within the approximately 1.0−2.0 kcal/mol deviation between G2 and G2(MP2) theory and experiment that has been reported for many test cases.[21] A calculation for $E_0 = 9.0$ kcal mol^{-1} is also shown in Figure 3, and with the other calculations indicates the sensitivity of the rate coefficient to E_0. It would also be possible to hold E_0 fixed at 8.0 kcal mol^{-1} and vary the collision parameters to fit the data. Taking the simple collisional efficiency approach, this would require about a factor of 3 decrease in the product of collision frequency and collisional efficiency. However, the calculated values of collisional efficiencies (β) listed in Table 6 are commensurate with literature values of β[26] for similar molecules, and large changes in the Lennard-Jones parameters would be required to force a fit.

Figure 4 shows an Arrhenius plot at 10 Torr. The line represents k_1(calcd) for $E_0 = 8.5$ kcal/mol, and the symbols are the values of k_1(exp) at 10 Torr for the four temperatures from 265 k to 306 k at which the experiments were done. For the 8.5 kcal mol^{-1} barrier the calculated 10 Torr rate coefficients are in accord with experiment. Table 6 lists the calculated and experimental rate coefficients. The RRKM calculated values of k_1 at 265 and 289 K are within the experimental range, which is the average deviation of the k_1 values determined by two different methods of data analysis.[17] At 280 K the RRKM value differs from the mean experimental value by 25%, and at 306 K the difference is only 12%. Arrhenius expressions for the calculations and the experiments (linear least squares, 2σ errors) are given by eqs 4 and 5.

$$k_{1,10\text{Torr}}(\text{calcd}) = 6 \times 10^8 \exp[-4080/T]\ \text{s}^{-1} \quad (4)$$

$$k_{1,10\text{Torr}}(\text{exptl}) = (7.7 \pm 2.3) \times 10^9 \exp[-(4803 \pm 722)/T]\ \text{s}^{-1} \quad (5)$$

The calculated 10 Torr E_a/R in eq 4 is at the low extreme of the experimental uncertainty of 722 cal/mol shown in eq 5, and the A-factors differ by a factor of 13. The difference can be attributed to the experimental value of k_1 at 265 K, which has an experimental deviation of ±45%. If k_1 is taken to be at the upper limit of the experimental range, 129 s^{-1}, the experimental value of E/R becomes about 4300 K, and A becomes about 1.4 × 10^9 s^{-1}, in much better agreement with the RRKM calculations.

The RRKM calculated temperature dependence of k_1 at the low and high-pressure limits can be expressed as

$$k_{1,0}(T) = 2.2 \times 10^{-9} \exp[\text{-}4153/T]\text{cm}^3\ \text{molecule}^{-1}\ \text{s}^{-1} \quad (6)$$

$$k_{1,\infty}(T) = 5.8 \times 10^{13} \exp[-4734/T]\ \text{s}^{-1} \quad (7)$$

TABLE 6: RRKM Calculation Results at Different Temperatures

	265 K	280 K	289 K	306 K
$k_{1,10\ \mathrm{Torr}}$ (s^{-1})	123	282	445	969
$k_{1,\mathrm{exp\ 10\ Torr}}$	89 ± 40	376 ± 75	419 ± 117	1104 ± 97
$k_{1,700\mathrm{Torr}}$ (s^{-1})	8.51×10^{3}	1.96×10^{4}	3.08×10^{4}	6.72×10^{4}
$k_{1,0}$ (cm^3 molecule^{-1} s^{-1})	3.24×10^{-16}	7.79×10^{-16}	1.27×10^{-15}	2.92×10^{-15}
$k_{1,\infty}$ (s^{-1})	1.03×10^{6}	2.66×10^{6}	4.49×10^{6}	1.11×10^{7}
β	0.417	0.398	0.387	0.368

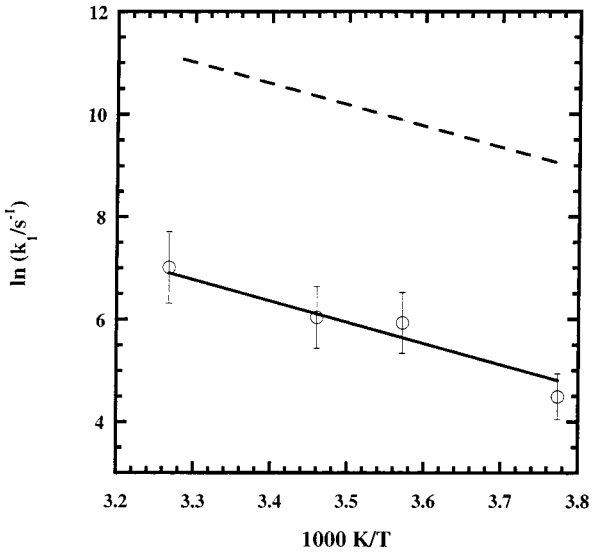

Figure 4. Arrhenius plots of k_1 at 10 and 700 Torr.) Experimental data at 10 Torr. (- -) Least-squares fit to data; (—) RRKM calculation at 10 Torr. (— —) RRKM calculation at 700 Torr.

Rate coefficients for Cl-atom elimination predicted by the ab initio/RRKM calculations are smaller than those for HCl elimination because of the larger barrier height. For $E_0 = 10.51$ kcal/mol, the high and low-pressure limit rate coefficients are $k_{2\infty} = 4.81 \times 10^{13} \exp[-5709/T]$ s^{-1} and $k_{2,0} = 7.12 \times 10^{-9} \exp[-5299/T]$ cm^3 $molecule^{-1}$ s^{-1}. The predicted relative rate coefficient for reactions 2 and 1 are $k_{2\infty}/k_{1\infty} = 3.2 \times 10^{-2}$ at 300 K and 9.9×10^{-3} at 220 K, and $k_{2,0}/k_{1,0} = 7.1 \times 10^{-2}$ at 300 K and 1.8×10^{-2} at 220 K. If E_0 is 11.2 kcal/mol,[13] these ratios will be even smaller. Thus Cl-atom elimination is predicted to make only a small contribution to the atmospheric chemistry of CH_2ClO. Small k_2/k_1 ratios must also explain the absence of experimental evidence for C−Cl bond breaking at ambient temperature and below.

4. Discussion

4.1. Ab Initio Calculations. Understanding the unimolecular dissociation of CH_2ClO is complicated by the presence of a low-lying excited state. The CH_2ClO radical belongs to point group C_S, and the electronic ground state is $^2A''$. A $^2A'$ excited state is formed by excitation of one of the $(2p_{x_O})^2$ nonbonding electrons into the singly occupied (in the ground state) $(2p_{y_O})$ orbital. In this reference frame the $x-z$ plane bisects the HCH bond angle and contains the C−O sigma bond. The $^2A'$ state is the low-lying excited state predicted to be nearly 7 kcal mol^{-1} above the ground state by both the G2 and G2MP2 calculations. The ground states of the products of reaction 1 are $HCl(\tilde{X}^1\Sigma^+)$ and $HCO(\tilde{X}^2A')$. These both correlate with A′ in point group C_S,[27] that is, with $CH_2ClO(\tilde{A}^2A')$, the first excited state of the reactant. The ground state, $CH_2ClO(\tilde{X}^2A'')$, correlates with excited $^1\Sigma^-$ states of HCl and $^2A''$ states of HCO, but these states are far too energetic to be formed at atmospheric temperatures. The HCl elimination transition state has no symmetry (see Table 1), belongs to point group C_1 and is a ^2A state. The formation of ground-state products may occur on an adiabatic surface that is a shoulder of a conical intersection[28] formed here by the crossing of the $^2A''$ and $^2A'$ CH_2ClO surfaces. The reaction is fully spin allowed.

A similar situation exists for C−Cl dissociation. The $H_2C(O)$ product belongs to point group C_{2v}. The $^2A''$ ground state of CH_2ClO correlates with A_2 states from C_{2v}, and the $^2A'$ excited-state correlates with A_1 states from C_{2v}. The ground state of $H_2C(O)$ is $^1A_1$, and the first two excited states are $^3A_2$ and $^1A_2$. The ground $^2A''$ state of CH_2ClO correlates with excited states of $H_2C(O)$, and the $^2A'$ excited state of CH_2ClO correlates with the ground state of $H_2C(O)$. Thus C−Cl bond breaking from the ground state of CH_2ClO to give ground-state products may also occur on an adiabatic surface that is a shoulder of a conical intersection. As shown above, the C−Cl bond breaking transition state belongs to point group C_1 and is a ^2A state.

Reaction path following calculations show that the energy along the reaction path for both reactions 1 and 2 decreases smoothly from the corresponding transition state structure toward the ground states of both the reactant and the products. The transition states for both HCl and C−Cl elimination correspond to saddle points with one imaginary frequency. The HCl and C−Cl elimination reaction paths are consistent with reactions occurring on adiabatic surfaces that may be formed as described above. The thermal population of CH_2ClO $(\tilde{A}^2A')$ at 300 K, using an excitation energy of 6.95 kcal/mol, is less than 10^{-5} of the ground-state population. Furthermore, the density of internal energy states in the vicinity of the barrier height is smaller in the excited state than in the ground state. These factors argue that the contribution of CH_2ClO $(\tilde{A}\ ^2A')$to the reaction rate is negligible at atmospheric temperatures.

Wang et al.[13] have calculated $E_0 = 11.2$ kcal/mol for C−Cl bond scission by G2(MP2) theory. The reason for the discrepancy with $E_0 = 10.5$ kcal/mol reported in Table 4 of this work, as mentioned above, is unknown. Hou et al.[29] later found a transition state for HCl elimination from CH_2ClO, although details have not been published. To locate this transition state Hou et al.[29] found that is was necessary to do geometry optimizations at MP2/6-31G(d,p), as we also found independently.[30] They reported that the HCl elimination barrier is 10.9 kcal/mol at G2(MP2), somewhat larger than the 8 kcal/mol that we obtained by G2(MP2) theory. If the difference in barrier height for reactions 1 and 2 were as small as 0.3 kcal mol^{-1}, both reactions 1 and 2 should be observed at 300 K, contrary to experiment.

The G2 and G2(MP2) calculations show that the C−Cl bond scission barrier is similar to C−Cl bond breaking barriers in other halogenated methoxy radicals. The reason that Cl release has not been experimentally observed is not that it has an especially high barrier, but that most experiments have been done at relatively low temperatures, and the RRKM calculations reported below show that the HCl barrier is enough lower that reaction 2 cannot compete with reaction 1. However, in reaction systems where CH_2ClO is formed at significantly higher

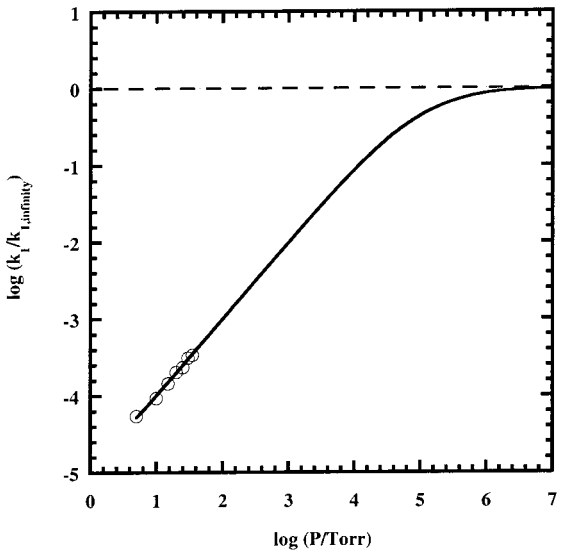

Figure 5. Pressure dependence of k_1 at 289 K.) Experimental data at 289 K. (—) 289 K RRKM calculation.

temperatures, such as oxidative pyrolysis of CH_3Cl, both reactions 1 and 2 would be expected to be important.

Sun and Bozzelli have recently published the results of a computational investigation of the thermochemistry of halogenated methanols and methoxy radicals.[33] For CH_2ClO they reported $\Delta H°_{f\ 298} = -5.13 \pm 2.18$ kcal/mol on the basis of DFT, CBSQ, and QCISD(T) calculations, in combination with six isodesmic reactions. We have estimated the enthalpy of formation of CH_2ClO in the present work solely from the thermally corrected G2 energies of CH_2ClO and the elements from which it is formed. The calculations give $\Delta H°_{f298}(CH_2ClO) = -6.6$ kcal mol^{-1}, in excellent agreement with Sun and Bozzelli, and $\Delta H°_{f0}(CH_2ClO) = -3.6$ kcal mol^{-1}.

4.2. RRKM Calculated Falloff. Figure 5 shows the calculated pressure dependence of k_1 from about 1 to 10^7 Torr at 289 K, along with the data from ref 16. The plot reiterates that experiment and calculation are in good agreement, shows that the experimental data are well down the falloff curve, and suggests that the data are very close to the low-pressure limit, as we have argued previously.[17] Figure 5 also shows that at 289 K the high-pressure limit is not closely approached until pressures in the vicinity of 10^7 Torr and above are reached. The extreme pressure of the high-pressure limit and the wide pressure range of the unimolecular falloff are characteristic of reactions with low energy barriers. The falloff curve for Cl elimination from CH_2ClO reported by Catoire et al.,[12] using RRKM parameters from MNDO calculations (which give a barrier of 20.6 kcal/mol), also shows a very broad falloff. Another example, which shows the effect of a low barrier on a larger molecule is the dissociation of $CF_2ClO_2NO_2$. The high-pressure limit of this reaction, for which $E_{a\infty} = 23.6$ kcal/mol, is approached above 20 atm. and the unimolecular rate coefficient decreases by about 2 orders of magnitude at a few Torr.[31] The CH_2ClO radical, with a barrier of only about 8 kcal/mol for the HCl channel, and being only a five-atom molecule, is an extreme case of this kind of behavior.

The calculated value of $A_{1\infty}$, 5.8×10^{13} s^{-1}, can be compared with $A_{1\infty} = 2.33 \times 10^{13}$ s^{-1}, calculated by the MNDO method.[12] These *A*-factors are considerably larger than the estimate of 10^9-10^{10} s^{-1} made by Wallington et al.[15] for $A_{1\infty}$, and are in accord with the expected "normal" range of preexponential factors for tight transition states. Wallington et al.[15] made their estimate on the basis of 700 Torr experimental data, and an assumption that the 700 Torr rate coefficient is no more than a factor of 2 from the high-pressure limit. A high-pressure *A*-factor as small as 10^9-10^{10} s^{-1} is unlikely, even if the reaction were nonadiabatic. Using the RRKM model to calculate the 700 Torr Arrhenius expression gives eq 8.

$$k_{1,calcd}(700\ \text{Torr}) = 5.2 \times 10^{10} \exp[-4140/T]\ \text{s}^{-1} \quad (8)$$

This shows that the 700 Torr estimate of the preexponential factor made by Wallington et al.[15] is actually quite good. The small numerical value is due to the unimolecular falloff, which according to Figure 5 is substantial at 700 Torr. In fact, eqs 7 and 8 predict that at 296 K $k_1(700\ \text{Torr})/k_{18} = 6.5 \times 10^{-3}$.

The RRKM calculated value of $E_{1\infty} = 9.4$ kcal mol^{-1} and the calculated 700 Torr activation energy of 8.2 kcal mol^{-1} are both within the uncertainty of the estimate of $E_{1\infty} = 8.6 \pm 1.9$ kcal mol^{-1} made by Wallington et al.[15] on the basis of 700 Torr data. The expected pressure dependence of the activation energy is revealed by the RRKM calculations, and is, in contrast with the pressure dependence of the *A*-factor, relatively insensitive to pressure. Thus the 1.9 kcal mol^{-1} uncertainty in the 700 Torr estimate embraces both the 700 Torr and high-pressure limit calculations of the activation energy.

4.3. The Relative Rate Coefficient. Wallington et al.[15] have reported the temperature dependence of the relative rate coefficient for reactions 1 and 3 at 700 Torr total pressure.

$$k_3/k_1 = 5.6^{+33}_{-4.9} \times 10^{-23} \exp[(3300 \pm 600)/\text{T}]\ \text{cm}^3\ \text{molecule}^{-1} \quad (9)$$

Combining the RRKM predicted rate coefficient for reaction 1 at 700 Torr from eq 8 with the experimental determination of the rate coefficient for reaction 3, $k_3 = (2.0 \pm 0.7) \times 10^{-12} \exp[-(934 \pm 128)/\text{T}]$ cm^3 molecule^{-1} s^{-1} [17] gives

$$(k_3/k_1) = 3.8 \times 10^{-23} \exp[3216/T]\ \text{cm}^3\ \text{molecule}^{-1} \quad (10)$$

in good agreement with Wallington et al.[15] Kaiser and Wallington[14] reported $k_3/k_1 = 5 \times 10^{-18}$ cm^3 molecule^{-1} at 296 K and 700 Torr, which can be compared with $k_3/k_1 = 3.9 \times 10^{-18}$ from eqn 4 and $k_3/k_1 = 1.98 \times 10^{-18}$ cm^3 molecule^{-1} from eq 5, both calculated at 296 K. The disparity between the largest and smallest values is a factor of 2.5, but the average of the three values is $(3.6 \pm 1.5) \times 10^{-18}$ cm^3 molecule^{-1}, showing a reasonable average deviation. Thus all of the 700 Torr data are in reasonable agreement.

Kaiser and Wallington[14] have reported a Troe fit to their pressure dependent [CO]/[HC(O)Cl] ratios at 296 K, from which it can be inferred that k_1 decreases by about a factor of about 20 between 700 and 20 Torr. The RRKM calculations reported here also predict that k_1 decreases by a factor of 20 over the same pressure range. Thus the extent of falloff is in very good agreement, and our earlier statement[15] about discrepancies in the falloff should be disregarded.

4.4. HCl Elimination from CH_2ClO in the Atmosphere. With the pressure and temperature dependence of k_1 from this work and ref 17, and the temperature dependence of k_3 from ref 16, the ratio of the rate of reaction 1 to reaction 2 can be calculated as a function of altitude in the atmosphere.

$$r_1/r_3 = k_1(T,P)/k_3(\text{T})[\text{O}_2] \quad (11)$$

At ground level ($T = 289$ K; $P = 760$ Torr), $r_1/r_3 = 2.5 \times 10^{-2}$. The rate ratio decreases with increasing altitude because the activation energy of reaction 1 is greater than the activation

energy of reaction 3, and k_1 decreases with decreasing pressure. At 30 km r_1/r_3 has decreased to 6.0×10^{-4}. Thus, HCl elimination due to the thermal reaction plays at most a minor role in the atmospheric chemistry of the CH_2ClO radical, accounting for only 2.5% of its loss near the surface, and lesser amounts as altitude increases. This corroborates the finding of Kaiser and Wallington[14] that in the atmosphere the dominant path for loss of thermal CH_2ClO radicals is reaction with O_2. However, evidence has been found from experiments at 296 K and 700 Torr that when CH_2ClO is formed by reaction of CH_2ClO_2 with NO a substantial fraction of the chloromethoxy radicals are chemically activated.[32] The chemically activated CH_2ClO decompose more rapidly than ground-state radicals and provide an additional path for removal of CH_2ClO. In the atmosphere this would mean enhanced HCl elimination over that due to the purely thermal reaction (as calculated by eq 11). In contrast with thermal unimolecular reactions, the decomposition of chemically activated molecules increases with decreasing pressure, so that the HCl (and possibly Cl loss also) formation will increase with increasing altitude. Further work on the oxidation of CH_3Cl in the presence of NO, particularly on the effect of pressure, are needed to address this issue.

Acknowledgment. This research was supported by NASA Upper Atmosphere Research Program under the grant NASA/NAG5-3980. Allocation of CPU time for the IBM SP supercomputer by the Supercomputing Institute for Digital Simulation and Advanced Computation at the University of Minnesota is gratefully appreciated. The authors also thank professors Donald Truhlar and Christopher Cramer for helpful discussions.

References and Notes

(1) Rayez, J. C.; Rayez, M. T.; Halvick, P.; Duguay, B.; Lesclaux, R.; Dannenberg, J. J. *Chem. Phys*. **1987**, *116*, 203.
(2) Rayez, J. C.; Rayez, M. T.; Halvick, P.; Duguay, B.; Dannenberg, J. J. *Chem. Phys*. **1987**, *118* 265.
(3) Li, Z.; Francisco, J. S, *J. Am. Chem. Soc.* **1989**, *111*, 5660.
(4) Lesclaux, R.; Dognon, A. M.; Caralp, F. *J. Photochem. Photobiol*. **1987**, *41*, 1.
(5) Simonaitis, R. Proc. *NATO Advanced Study Institute on Atmospheric Ozone*; Nicolet, M., Aikin, A. C., Eds.; Algarve, Portugal, 1979; p 501.
(6) Carr, R. W.; Peterson, D. G.; Smith, F. K. *J. Phys. Chem*. **1986**, *90*, 607.
(7) Sanhueza, E. *J. Photochem*. **1980**, *14*, 157.
(8) Hautecloque, S. *J. Photochem*. **1977**, *7*, 325.
(9) Wu, F.; Carr, R. W. *J. Phys. Chem*. **1992**, *96*, 1743.
(10) Sanhueza, H.; Heicklen, S. *J. Phys. Chem*. **1975**, *79*, 7.
(11) Niki, H.; Maker, P. D.; Savage, C. M.; Breitenbach, L. P. *J. Chem. Kinet*. **1980**, *12*, 1001.
(12) Catoire, V. A.; Lesclaux, R.; Lightfoot, P. D.; Rayez, M. T. *J. Phys. Chem*. **1994**, *98*, 2889.
(13) Wang, B.; Hou, H.; Gu, Y. *J. Phys. Chem. A* **1999**, *103*, 2060.
(14) Kaiser, E. W.; Wallington, T. J. *J. Phys. Chem*. **1994**, *98*, 5679.
(15) Wallington, T. J.; Orlando, J. J.; Tyndall, G. S. *J. Phys. Chem*. **1995**, *99*, 9437.
(16) Wu, F.; Carr, R. W. *Chem. Phys. Lett.* **1999**, *305*, 44.
(17) Wu, F.; Carr, R. W. *J. Phys. Chem.* A **2001**, *105*, 1423.
(18) Frisch, M. J.; Trucks, G. W.; Schlegel, H. B.; Gill, P. M. W.; Johnson, B. G.; Robb, M. A.; Cheeseman, J. R.; Keith, T.; Petersson, G. A.; Montgomery, J. A.; Raghavachari, K.; Al-Laham, M. A.; Zakrzewski, V. G.; Ortiz, J. V.; Foresman, J. B.; Cioslowski, J.; Stefanov, B. B.; Nanayakkara, A.; Challacombe, M.; Peng, C. Y.; Ayala, P. Y.; Chen, W.; Wong, M. W.; Andres, J. L.; Replogle, E. S.; Gomperts, R.; Martin, R. L.; Fox, D. J.; Binkley, J. S.; Defrees, D. J.; Baker, J.; Steward, J. P.; Head-Gordon, M.; Gonzalez, C.; Pople, J. A. *GAUSSIAN 94*, revision D.2; Gaussian, Inc.: Pittsburgh, PA, **1995**.
(19) Foresman, J. B.; Frisch, Æ., *Exploring Chemistry with Electronic Structure Methods*, 2nd ed.; Gaussian, Inc.: Pittsburgh, PA, 1996.
(20) Curtiss, L. A.; Raghavachari, K.; Trucks, G. W.; Pople, J. A. *J. Chem. Phys*. **1991**, *94*, 7221.
(21) Curtiss, L. A.; Raghavachari, K.; Pople, J. A. *J. Chem. Phys*. **1993**, *98*, 1293.
(22) Curtiss, L. A.; Redfern, P. C.; Smith, B. J.; Radom, L. *J. Chem. Phys*. **1996**, *104*, 5148.
(23) Gilbert, R. G.; Smith, S. C.; Jordam, M. J. T. UNIMOL Program Suite (Calculation of Falloff Curves for Unimolecular and Recombination Reactions). 1993. Available from the authors.
(24) Gilbert, R. G.; Smith, S. C. *Theory of Unimolecular and Recombination Reactions*; Blackwell Scientific Publications: Oxford, 1990.
(25) Forst, W. *Theory of Unimolecular Reactions*; Academic Press: New York, 1973; p 177.
(26) Oref, I.; Tardy, D. C. *Chem. Rev*. **1990**, *90*, 1407.
(27) Okabe, H. *Photochemistry of Small Molecules*; Wiley-Interscience: New York 1978; pp 71−77.
(28) Truhlar, D. G. *J. Chem. Soc., Faraday Trans.* **1994**, *90*, 1614. Allison, T. C.; Lynch, G. C.; Truhlar, D. G.; Gordon, M. S. *J. Phys. Chem.* **1996**, *100*, 13575.
(29) Hou, H.; Wang, B.; Gu, Y. *J. Phys. Chem*. **1999**, *103*, 8075.
(30) Wu, F.; Carr, R. W. Presentation at the XXIII Informal Conference on Photochemistry, Pasadena, California, May 10−15, 1998.
(31) Xiong, J. Q.; Carr, R. W. *J. Phys. Chem*. **1994**, *98*, 9811.
(32) Bilde, M.; Orlando, J. J.; Tyndall, G. S.; Wallington, T. J.; Hurley, M. D.; Kaiser, E. W. *J. Phys. Chem*. **1999**, *103*, 3963.
(33) Sun, H.; Bozzelli, J. W. *J. Phys. Chem. A* **2001**, *105*, 4504.